

Simulating Complex Dynamics In Intermediate And Large-Aspect-Ratio Convection Systems

Ming-Chih Lai

Department of Mathematics, Chung Cheng University, Minghsiung, Chiayi 621, Taiwan

Keng-Hwee Chiam and M.C. Cross

Department of Physics, California Institute of Technology, Pasadena, CA 91125

Henry Greenside

Department of Physics, P. O. Box 90305, Duke University, Durham, NC 27708-0305

Abstract

Buoyancy-induced (Rayleigh-Bénard) convection of a fluid between two horizontal plates is a central paradigm for studying the transition to complex spatiotemporal dynamics in sustained nonequilibrium systems. To improve the analysis of experimental data and the quantitative comparison of theory with experiment, we have developed a three-dimensional finite-difference code that can integrate the three-dimensional Boussinesq equations (which govern the evolution of the temperature, velocity, and pressure fields associated with a convecting flow) efficiently in large box-shaped domains with experimentally appropriate lateral boundary conditions. We discuss some details of this code and present two applications, one to the occurrence of quasiperiodic dynamics with as many as 5 incommensurate frequencies in a moderate-aspect-ratio 10×5 convection cell, and one to the onset of spiral defect chaos in square cells with aspect ratios varying from $\Gamma = 16$ to 56.

Introduction

A frontier of great importance for DOE-related research is the study of sustained nonequilibrium dynamical systems, for which imposed external fluxes of energy and matter can lead to states that vary temporally and spatially in a complex way [1]. Despite the collaboration of theorists, computational scientists, and experimentalists over the last thirty years and despite the great need to solve numerous practical engineering problems, many basic questions about sustained nonequilibrium states remain unanswered. Researchers would like to know what possible states can occur for specified external fluxes, how to predict when one state will change into another as some parameter is varied, how transport of energy and matter depends on the spatiotemporal structure of a state, and whether one can select particular states by appropriate external perturbations so as to optimize a system for a particular goal. While experiments and simulations have been useful in suggesting what possibilities can occur (e.g., the surprising experimental discovery of the spiral defect chaos state [2], a numerical example of which is shown below in Fig. 3), there remains a great need to develop a stronger theoretical and conceptual foundation that can unify the many observations and that can improve both experimental and computational investigations.

Perhaps the simplest and best idealized experimental system for exploring basic questions and principles of nonequilibrium systems is Rayleigh-Bénard convection, which has become an experimental and theoretical paradigm for many researchers [1]. A Rayleigh-Bénard experiment consists of a thin layer of fluid confined between two horizontal spatially-uniform constant-temperature metal plates such that the bottom plate is maintained at a constant higher temperature than the upper plate. As the temperature difference (or its dimensionless equivalent, the Rayleigh number R) is increased in successive constant steps, the fluid first makes a transition from a motionless structureless state to cellular overturning convection rolls and then to ever more complex dynamical states which eventually become nonperiodic in space and time. Convection has significant advantages over other experimental systems in having static homogeneous boundary conditions, in having no net flow of fluid through the system, in allowing precise and reproducible experiments with

good visualization, and in being amenable to a quantitative mathematical description through the so-called Boussinesq equations.

In this paper, we report applications of a new computer code to two intriguing convection experiments. The code is the first of several being developed and applied by a Caltech-Duke collaboration whose long-term goal is to understand convection phenomena more quantitatively, especially in the large-aspect-ratio limit (cells whose widths are large compared to their depths) which experiments have shown to be of great interest even close to the onset of convection, where analytical progress is most likely to be possible [1]. Our code differs from some other recently developed codes [3] primarily through the inclusion of experimentally appropriate lateral boundary conditions (rather than periodic boundary conditions) on the velocity and temperature fields so that the forcing due to lateral boundaries can be taken into account. In the following sections, we give a brief summary of the code followed by a discussion and demonstration of how the code can provide new insights about two poorly understood experimental phenomena, the occurrence of dynamics with many incommensurate frequencies in a moderate-aspect ratio convection cell first observed by Walden et al [4] and the onset of spiral defect chaos in domains of varying size (which has not yet been studied experimentally). These results provide new and detailed examples of the substantial influence of lateral boundaries on nonequilibrium dynamics.

Numerical Integration Of The 3D Boussinesq Equations

Since technical details of our numerical algorithm will be available elsewhere [5], we provide only some motivation for and highlights of our numerical method. The goal is to integrate the five coupled three-dimensional nonlinear partial differential equations known as the Boussinesq equations which state (under certain assumptions not given here) the local conservation of momentum, energy, and mass for parcels of fluid subjected to buoyancy forces. By scaling time, space, and field magnitudes in appropriate ways, one can write the Boussinesq equations in the following dimensionless form:

$$\partial_t \mathbf{u} = -\mathbf{u} \cdot \nabla \mathbf{u} - \nabla p + \sigma \nabla^2 \mathbf{u} + \sigma R T \hat{z}, \quad (1)$$

$$\partial_t T = -\mathbf{u} \cdot \nabla T + \nabla^2 T, \quad (2)$$

$$\nabla \cdot \mathbf{u} = 0, \quad (3)$$

where $\mathbf{u}(t, \mathbf{x}) = (u_x(t, \mathbf{x}), u_y(t, \mathbf{x}), u_z(t, \mathbf{x}))$ is the velocity field at time t and position $\mathbf{x} = (x, y, z)$, $T(t, \mathbf{x})$ is the temperature field, $p(t, \mathbf{x})$ is the pressure field, σ is the fluid's Prandtl number which is assumed to be independent of temperature and so a constant, and R is the Rayleigh number which is the key parameter that is varied in most experiments and simulations, usually with all other parameters held fixed. In this paper, we study these equations in a simple box geometry of dimensions $\Gamma_x \times \Gamma_y \times 1$; the quantities Γ_x and Γ_y are ratios of lateral widths to the unit fluid depth and are called aspect ratios. Since the fluid is confined by stationary material walls, the velocity vanishes at these walls which provides the following boundary condition on \mathbf{u} :

$$\mathbf{u} = 0 \quad \text{on all walls.} \quad (4)$$

With our rescaled variables, the constant temperature boundary conditions on the bottom and top plates ($z = 0$ and $z = 1$ respectively) are simply

$$T(t, x, y, 0) = 1 \quad \text{and} \quad T(t, x, y, 1) = 0. \quad (5)$$

The temperature field T satisfies an additional boundary condition on the lateral walls which, for this paper, we take to be a no-flux condition corresponding to a perfect thermal insulator

$$\partial_n T = \hat{\mathbf{n}} \cdot \nabla T = 0 \quad \text{on lateral walls,} \quad (6)$$

where $\hat{\mathbf{n}}$ is the normal unit vector at a given point on the wall. However, the code is more general and can treat thermal boundary conditions that interpolate between conducting and insulating sidewalls.

The numerical challenge is to integrate these equations and boundary conditions efficiently and accurately over long time intervals in large cells of simple geometry; boxes and cylinders cover nearly all the experimental cases while a box with periodic sidewalls is useful for comparing with theory. Rayleigh-Bénard convection

is so important that many numerical methods have been developed and tried over the years although, somewhat unfortunately, most of these methods have not been compared with each other to determine which best achieves a practical balance of efficiency, accuracy, ease of programming, and parallel scalability on some specific computer architecture. Because our interest is to study fundamental questions in simple cell geometries, we chose not to use finite element or spectral element methods whose main strengths are the ability to handle irregular boundaries. Because our short term needs are for modest accuracy, simplicity and flexibility of coding, and good parallel scaling on Beowulf-style computers, we chose second-order-accurate finite-difference approximations on Cartesian meshes instead of spectral methods.

Our code uses a traditional time-splitting method in which higher-order linear operators are advanced implicitly in time and lower-order nonlinear terms are advanced explicitly [5], achieving at each time step an overall accuracy of second order in time. The incompressibility condition $\nabla \cdot \mathbf{u} = 0$ is treated by a standard projection method [6] in which the momentum conservation equations are used to update the current velocity $\mathbf{u}(t, \mathbf{x})$ to an intermediate field \mathbf{u}^* that is not divergence free, and then \mathbf{u}^* is “projected” onto a divergence-free field $\mathbf{u}(t + \Delta t, \mathbf{x})$ by solving a Poisson equation for the new pressure field. To advance one time step Δt , four 3D Helmholtz equations and one 3D Poisson equation must be solved with appropriate boundary conditions, and the solution of these linear equations constitute the most time consuming part of the code. For this first generation code, we used FISHPACK fast direct solvers (available through www.netlib.org) which are well suited for modest-aspect-ratio problems on single-processor Alpha workstations. Future codes will use parallel iterative methods which are also better suited for the non-constant-coefficient linear operators that arise in a cylindrical geometry.

Our code was innovative mainly through the use of *colocated* meshes, in which all field values and all operators of field values were evaluated on the same set of mesh points. For two- and three-dimensional fluid simulations of incompressible flow, empirical studies and some analysis have suggested that staggered meshes (in which scalar quantities are stored at the centers of grid boxes while vector components are stored on the faces or vertices of the boxes) were necessary to avoid numerical instabilities associated with the pressure [7]. Our colocated-mesh Boussinesq code proved to be numerically stable which led to a substantial reduction in the effort of writing and validating the code compared to a staggered-mesh code. For lack of space, we refer to our forthcoming paper for further details, e.g., how our code was validated and its efficiency and accuracy as a function of various parameters [5].

Applications

We now report on two preliminary applications of the above convection code. First we try to simulate an intriguing experiment [4] that goes to the heart of how chaotic behavior arises in a continuous medium, here through the occurrence of quasiperiodic states with as many as five incommensurate frequencies. The mystery to understand is the spatial structure of the different oscillations and their dependence on aspect ratio and Rayleigh number. Second, we investigate how the onset of spiral defect chaos state [2] depends on the aspect ratio Γ of a square box, which we increase in small successive increments. Varying the aspect ratio is difficult in laboratory experiments and these calculations demonstrate the usefulness of having quantitatively accurate codes to complement experiments.

Multi-Frequency Dynamics at Intermediate Aspect Ratios

Our first calculation was motivated by the experimental paper of Walden et al [4], which reported in 1984 the unexpected occurrence of spatiotemporal quasiperiodic states in a convecting flow with as many as five incommensurate frequencies. This result seemed to contradict one of the major mathematical insights of the time, a theorem of Newhouse, Ruelle, and Takens [8] which argued that chaotic behavior should be typically observed after at most three successive Hopf bifurcations since quasiperiodic dynamics with three or more incommensurate frequencies can be perturbed infinitesimally to become chaotic. Although the abstract mathematical arguments were difficult to interpret for laboratory experiments and despite clarifications of this theorem by later numerical simulations on simple map systems [9], it is still not understood how a physical continuous medium can develop so many independent oscillations or whether a physical mechanism can be identified for each independent frequency.

To make contact with this experiment, we have carried out the first (to our knowledge) simulations in a box-like domain with parameters nearly identical to those of the experiment. Thus we performed numerical integrations of the 3D Boussinesq equations in a cell of aspect ratio $9.5 \times 4.5 \times 1$, for a fluid with Prandtl number $\sigma = 3.5$ (corresponding to water with a mean temperature of 50°C) and over a comparable range of Rayleigh numbers up to $R = 20R_c$, where $R_c \approx 1708$ is the critical value for the onset of convection in an infinite-aspect-ratio cell. The most poorly justified approximation was our choice of laterally insulating sidewalls Eq. (6) since the real experiment had finitely conducting glass sidewalls between a copper bottom plate and sapphire upper plate. (The thermal diffusivities κ of copper, glass, sapphire, and water are respectively 1.20, 0.004, 0.113, and $0.00147 \text{ cm}^2/\text{sec.}$) A typical run used a resolution of $76 \times 36 \times 8$ points and a constant time step of $\Delta t = 0.001$. A run to collect 65,000 points took approximately 1.5 hours on a Compaq XP1000 workstation using a 667 MHz 264 Alpha chip with a 4 MB cache.

Some representative results are shown in Fig. 1. As the Rayleigh number R is increased in small steps, new incommensurate frequencies appear until, at $R/R_c = 17.5$, 5 incommensurate frequencies are observed just as in the experiment. The fact that these frequencies were incommensurate was supported by plotting (not shown) the ratios of frequencies corresponding to different peaks and observing that these ratios varied smoothly with R , i.e., no mode locking to a rational value took place. The numerical simulations did not

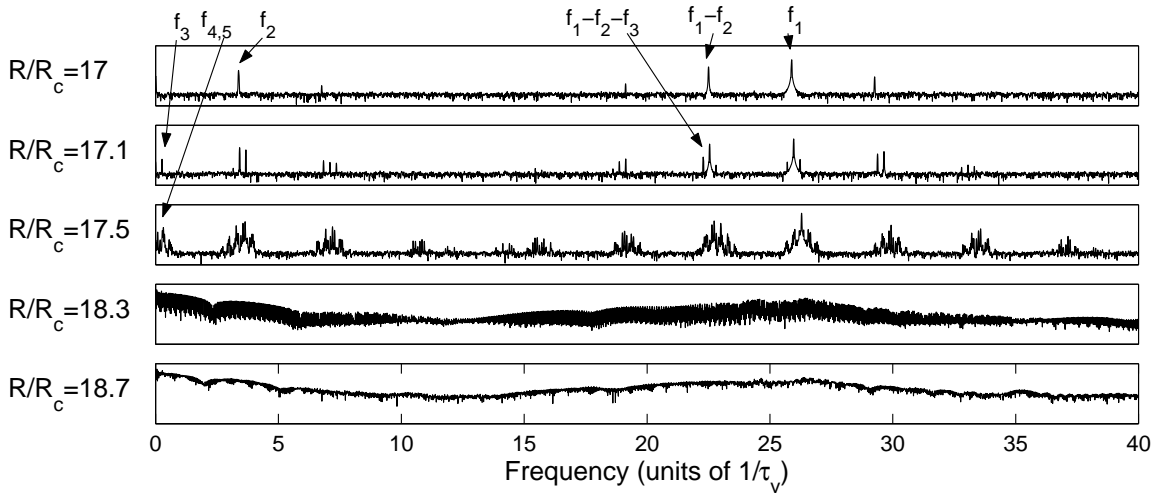


Figure 1: Power spectra $P(f)$ versus frequency f for five values of the Rayleigh number R over the range $17 \leq R/R_c \leq 18.7$ in a cell of aspect ratio $9.5 \times 4.5 \times 1$ and for a fluid of Prandtl number $\sigma = 3.5$. The top three panels show quasiperiodic motion with 2, 3, and 5 incommensurate frequencies respectively. The last two panels show spectra of chaotic dynamics with continuous broad-band features.

reproduce quantitatively the magnitude of the lower frequencies observed in experiment. For example, for the 4-frequency convection state, the simulation has a low frequency peak at $f_4 \approx 0.17$ which is about a factor of three smaller than that observed in the experiment. A first guess is that this discrepancy is a consequence of the convenient but experimentally inaccurate no-heat-flux boundary condition Eq. (6).

In related simulations, we have also explored how the dynamics depended on aspect ratio, a question which is difficult to explore experimentally. Fig. 2 shows several instantaneous convection patterns and the power spectra of the corresponding time-dependent states over the range $9.5 \leq \Gamma_x \leq 10.5$ with Γ_y and R held fixed. A surprising and new result is that small changes in Γ lead to dramatically different patterns and dynamics. Indeed, for the states of Fig. 2 and others not shown over this same range, one can identify time independent, periodic, quasiperiodic (with 3 and 4 frequencies), and chaotic dynamics. The spatiotemporal dynamics is evidently highly sensitive to small changes in the system geometry at these intermediate aspect ratios.

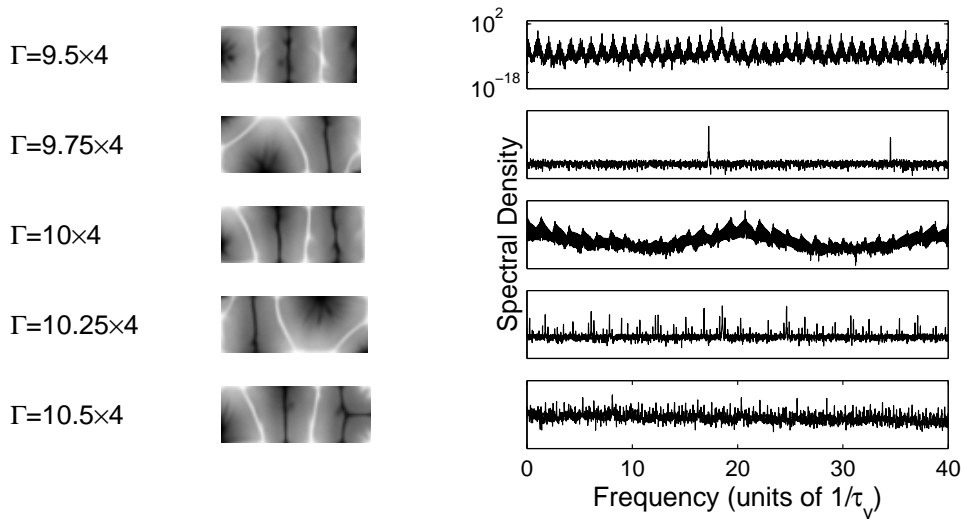


Figure 2: Changes in convection dynamics as the aspect ratio Γ_x is increased in small steps for fixed $\Gamma_y = 4$ and $R = 18R_c$. The left column of plots are instantaneous density plots of the temperature field at the midplane $z = 1/2$ with light regions corresponding to warm fluid, dark regions to cool fluid. The right column of plots are corresponding power spectra $P(f)$ calculated from time series of 65,536 values of the temperature at the midpoint of the cell. Rows 1, 3, and 5 are chaotic, row 2 is periodic, and row 4 is quasiperiodic with three independent frequencies.

Onset of Spiral Chaos

As the technology improved for exploring large-aspect-ratio convection dynamics, experimentalists made a remarkable discovery in 1993 [2] of an intricate spatiotemporal chaotic convecting flow in a cylindrical geometry near onset, a regime that previous experiments in smaller aspect ratios had suggested would show only simple convective patterns, and for which theory predicts that parallel time-independent convection rolls should be stable [10]. This *spiral defect chaos* state (so named because of the unexpected occurrence of rotating spiral structures) remains poorly understood seven years later and is now regarded by many convection researchers to be an especially important example of spatiotemporal chaos to understand. Intriguing and also poorly understood is the experimental observation that spiral defect chaos is observed only when the aspect ratio Γ of the cylindrical cell is sufficiently large, with the radius being at least 40 times the fluid depth.

Using the code described above, we have explored for the onset and properties of spiral defect chaos in finite cells with experimentally realistic lateral boundary conditions and with varying aspect ratio, although for a square rather than cylindrical geometry. Representative results for two different values of the reduced Rayleigh number $\varepsilon = (R - R_c)/R_c$ are shown in Fig. 3. For $\Gamma \leq 24$, the asymptotic dynamics are stationary while time-dependent states are observed for larger Γ , with spirals being observed only for the larger Rayleigh numbers. Spirals appear in square geometries for smaller aspect ratios than those of a cylindrical cell at the same reduced Rayleigh number.

As a first step towards quantifying and analyzing these complex patterns, we have calculated the time-averaged distribution $P(q)$ of local wave numbers q as a function of aspect ratio and Rayleigh number. Following a recent suggestion of Egolf et al [11], we estimated local wave numbers $q(t, x, y)$ from the ratio $-\nabla^2\theta/\theta$ where $\theta = \theta(t, x, y, 1/2)$ is the deviation of the temperature field T from its linear conducting profile, evaluated at the cell midplane $z = 1/2$. The distribution $P(q)$ was then obtained by averaging many instantaneous histograms of q over time. A compilation of the mean wave numbers \bar{q} associated with each wave number distribution is shown in Fig. 4, which shows rather remarkably that the trend for the variation of \bar{q} with R is nearly independent of the aspect ratio, and that \bar{q} decreases roughly linearly with increasing Rayleigh number up to $R/R_c \simeq 2$. Near the value $q - q_0 = -0.8$ (with q_0 the critical wave number at onset),

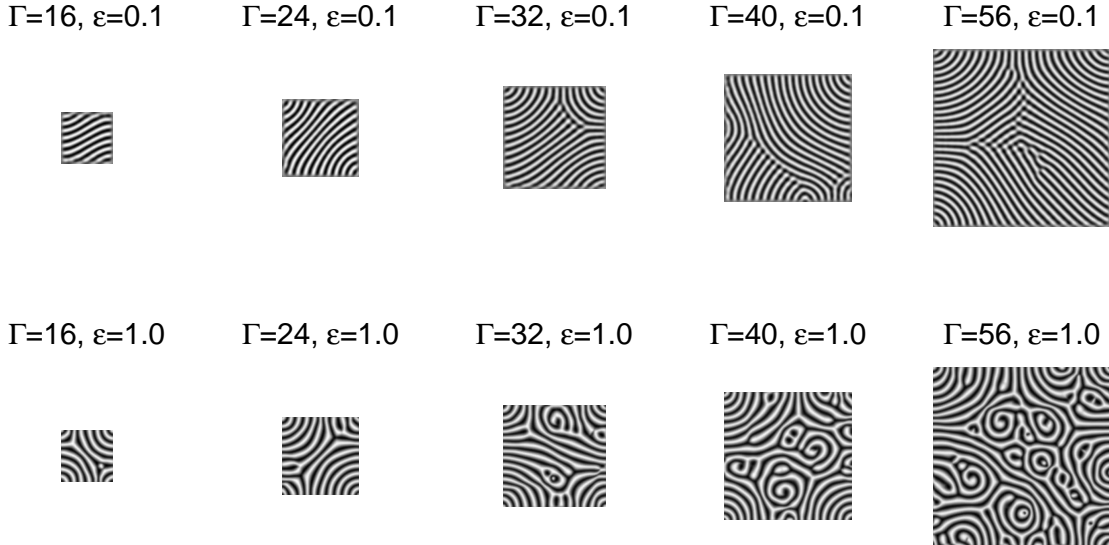


Figure 3: Instantaneous patterns observed in various aspect ratios for two values of the reduced Rayleigh number $\varepsilon = (R - R_c)/R_c$ and for a fixed Prandtl number of $\sigma = 0.96$, corresponding to the compressed CO_2 gas used in the experiments. The first two columns of states are time independent.

there is a dramatic change with \bar{q} becoming essentially independent of R . At this point, spiral defect chaos develops in the larger aspect ratio cells while the smaller cells are chaotic and lack spiral defects.

The average spatial disorder of each pattern can also be quantified by a correlation length ξ , which is defined here to be the inverse of the width of the distribution $P(q)$. The inset in Fig. 4 shows that ξ is also insensitive to the aspect ratio and obeys approximately a power law dependence $\varepsilon^{-1/2}$ which is the same as that predicted by the amplitude equation theory [1] (although the range of Rayleigh numbers in the plot is much larger than the range over which this theory might be expected to hold). A similar trend has again been noticed in cylindrical geometry experiments, although an experiment in a rectangular cell found a divergence at a nonzero value of ε .

The trend of $\bar{q}(\varepsilon)$ in Fig. 4, which has also been observed in cylindrical experiments, is far from that predicted theoretically by Cross and Newell [13], who argued that portions of circular rolls around a “focus singularity” such as those spanning the corners in the cells of Fig. 3 should lead to the selection of the same wave number q_f as that selected in concentric axisymmetric rolls [14]. The discrepancy is particularly striking in the simple structures seen at low values of ε such as Fig. 5, where theory [13] suggests that the focus singularities in the corners should determine the wave number over much of the system. One possible way in which arcs of rolls can act differently than complete circles is that arcs can drive a “mean flow”, which may then modify the wave number distribution. The mean flow is, roughly, the horizontal fluid flow integrated across the depth of the cell and cannot occur in axisymmetric (or straight) roll configurations because of the incompressibility of the fluid. The mean flow is known to be important in producing the skew-varicose instability and in suppressing the zigzag instability for Prandtl numbers of order unity.

Using the detailed knowledge provided by the code of the convection pattern, the wave number distribution, and the mean flow, we are able to assess for the first time the importance of the mean flow in producing the deviations of the measured wave number \bar{q} from q_f . Fig. 5 shows the distribution of the wave number field and corresponding mean flow. In regions towards the center of the cell where the mean flow is small, the wave number is indeed close to the predicted value $q_f = 3.1$. However circulating mean flow patterns develop in the cell corners and the wave numbers there are substantially reduced below q_f . A plot of the distribution $P(q)$ (not shown) indicates in fact that the *largest* q with significant probability is close to q_f but the spread of $P(q)$ to smaller values of q means that the *mean* \bar{q} is considerably below q_f . Given the characteristic form of the mean flows that form in the corners—consisting of two regions of counter-rotating vorticity—an analytic attack on this long standing question is an appropriate next step.

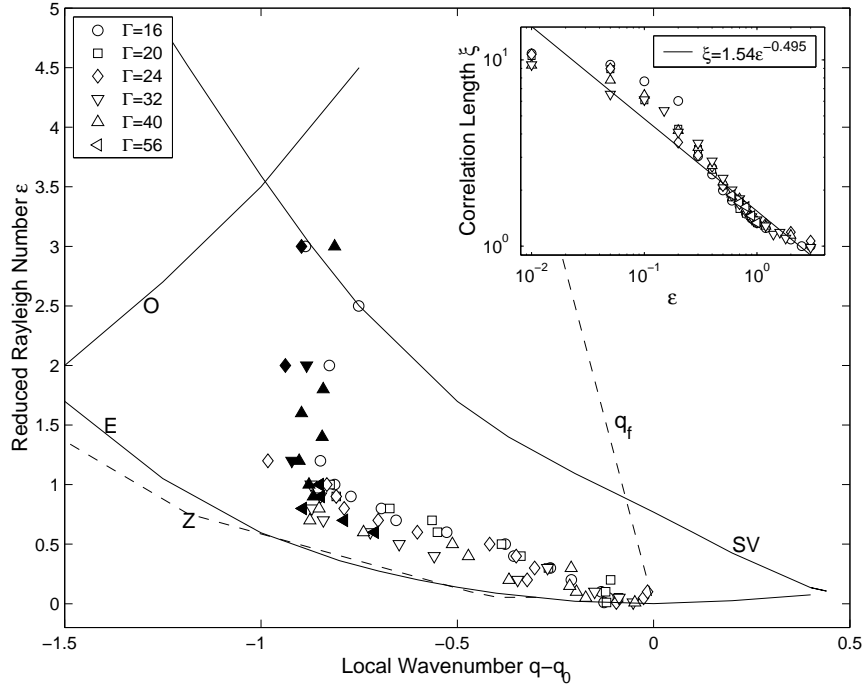


Figure 4: Plot of the deviation $\bar{q} - q_0$ of the mean wave number \bar{q} from the critical wave number $q_0 = 3.117$ as a function of the reduced Rayleigh number ϵ . Also shown are the instability boundaries [12] which limit the range for the ideal roll state in a laterally infinite geometry (SV=skew varicose; O=oscillatory; E=Eckhaus; Z=zigzag), and the wave number $q_f(\epsilon)$ that is selected in axisymmetric rolls. Solid symbols denote states where dynamic spiral defects are observed. The inset shows the correlation length ξ defined as the inverse of the width of the wave number probability distribution $P(q)$. The straight line has a slope 1/2 as would be predicted by the amplitude equation theory near threshold.

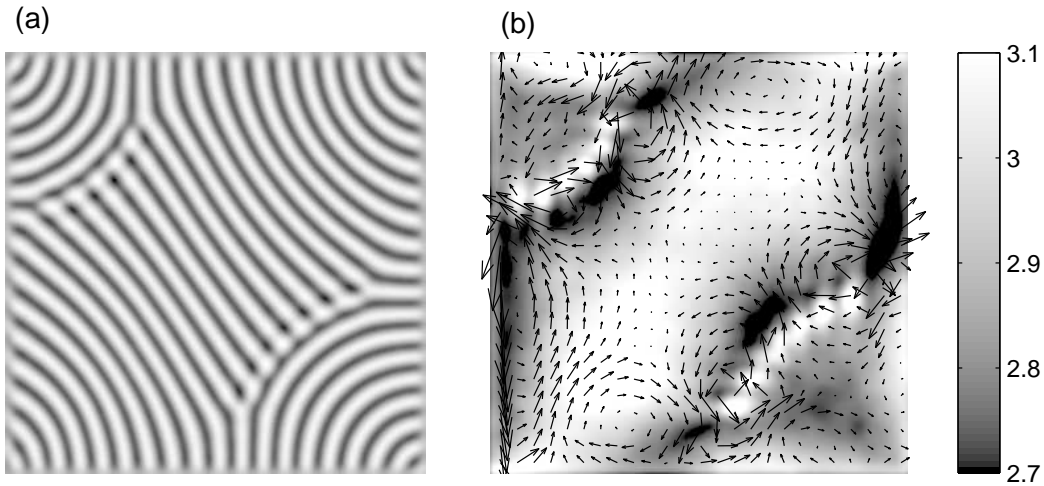


Figure 5: (a) Roll pattern and (b) wave number distribution (gray scale) at $R/R_c = 1.15$ in a cell of aspect ratio $\Gamma = 40$. The corresponding mean flow (arrows) was estimated by integrating the horizontal velocity components of \mathbf{u} vertically over the fluid depth. The maximum Euclidean norm of \mathbf{u} has the value 6.1 in units of d/t_v while the mean flow is much smaller, with a corresponding maximum magnitude of 0.12.

Conclusions

As initial applications of our intermediate- to large-aspect-ratio fluid convection code we have studied two aspects of the onset of chaotic dynamics. In both of these examples the role of the physical boundaries were found to play a vital role—in the intermediate aspect ratio by determining the basic structures about which dynamics develops, and in the large aspect ratio cell where the mean flows that form in the corners of the cell play an important roll in determining the wave number distribution—and so the physical issues are not accessible to previous codes where periodic boundary conditions are used. The preliminary results we present here suggest further directions to explore, both numerically and analytically.

Acknowledgements

This work was supported by the Engineering Research Program of the Office of Basic Energy Sciences at the Department of Energy, Grant DE-FT02-98ER14892. We also thank Paul Kolodner for useful discussions concerning the convection apparatus of Walden et al.

References

- [1] M. C. Cross and P. C. Hohenberg. Pattern formation outside of equilibrium. *Rev. Mod. Phys.*, 65(3):851–1112, 1993.
- [2] Stephen W. Morris, Eberhard Bodenschatz, David S. Cannell, and Guenter Ahlers. Spiral defect chaos in large-aspect-ratio Rayleigh-Bénard convection. *Phys. Rev. Lett.*, 71(13):2026–2029, September 1993.
- [3] W. Decker, W. Pesch, and A. Weber. Spiral defect chaos in Rayleigh-Bénard convection. *Phys. Rev. Lett.*, 73(5):648–651, 1994.
- [4] R. W. Walden, P. Kolonder, A. Passner, and C. M. Surko. Nonchaotic Rayleigh-Bénard convection with four and five incommensurate frequencies. *Phys. Rev. Lett.*, 53:242–245, 1984.
- [5] M. Lai and H. S. Greenside. An Efficient Colocated Mesh Projection Method for Simulating Large-Aspect-Ratio Rayleigh-Bénard Convection. To be submitted to the Journal of Computational Physics, 2000.
- [6] John B. Bell, Phillip Colella, and Harland M. Glaz. A second-order projection method for the incompressible Navier-Stokes equations. *J. Comp. Phys.*, 85:257–283, 1989.
- [7] Francis H. Harlow and J. Eddie Welch. Numerical calculation of time-dependent viscous incompressible flow of fluid with free surface. *Phys. Fluids*, 8(12):2182–2189, 1965.
- [8] Edward Ott. *Chaos in Dynamical Systems*. Cambridge U. Press, New York, 1993.
- [9] C. Grebogi, E. Ott, and J. A. Yorke. Attractors on an N -Torus: Quasiperiodicity Versus Chaos. *Physica D*, 15:354, 1985.
- [10] Reha. V. Cakmur, David A. Egolf, Brendan B. Plapp, and Eberhard Bodenschatz. Bistability and competition of spatiotemporal chaotic and fixed point attractors in Rayleigh-Bénard convection. *Phys. Rev. Lett.*, 79(10):1853–1856, 1997.
- [11] David A. Egolf, Llarion V. Melnikov, and Eberhard Bodenschatz. Importance of local pattern properties in spiral defect chaos. *Phys. Rev. Lett.*, 80(15):3228–3231, 1998.
- [12] F. H. Busse. Nonlinear properties of convection. *Rep. Prog. Phys.*, 41:1929–1967, 1978.
- [13] M. C. Cross and A. Newell. Convection patterns in large aspect ratio systems. *Physica*, 10D:299–328, 1984.
- [14] J. C. Buell and I. Catton. Wavenumber selection in large-amplitude axisymmetric convection. *Physics of Fluids*, 29:23–30, 1986.